An OH survey of very cold IRAS point sources

Te Lintel Hekkert, P.

Astron. Astrophys. 248, 209–220 (1991)

ASTRONOMY AND ASTROPHYSICS

An OH survey of very cold IRAS point sources

P. te Lintel Hekkert*

Sterrewacht Leiden, P.O. Box 9513, NL-2300 RA Leiden, The Netherlands

Received January 26, 1990; accepted January 11, 1991

Abstract. We present a survey of 84 IRAS point sources carried out using the Nançay radiotelescope at all four 18 cm transitions of the OH radical. The point sources have been selected on basis of their infrared colour temperatures of about 100 K; similar to the colour temperatures of known high velocity outflow sources (e.g. te Lintel Hekkert et al. 1988) and OHPN (Zijlstra et al. 1989).

We found emission and/or absorption of 13 sources: nine are compact H II regions or star formation regions and four are proto-planetary nebulae (hereafter PPN): Hen 3−1475, IRAS 18491−0207, OH 17.7−2.0 and IRAS 22036+5306. The OH 1667 MHz maser emission of the PPN IRAS 18491−0207 has a total velocity width of 200 km s^{-1}, the largest known in the OH line. IRAS 22036+5306 is the coldest IRAS point source, with an OH maser emission line profile resembling that of an OH/IR star. The discovery of 1720 MHz maser emission from the H II region K 3–35 could be explained by the H_2O dissociation pump for this maser transition as suggested by Andresen (1986).

The IRAS $f_{60\mu m}$ flux can be used as a discriminator between PPN and H II regions. The detected H II regions, which are associated with molecular clouds have $f_{60\mu m} > 1000$ Jy; the PPN have $f_{60\mu m}$ between 60 and 250 Jy. However, we detected two H II regions with $f_{60\mu m}$ below 60 Jy, which suggests that these are low luminosity objects and might be progenitors of low mass stars.

Key words: masers – stars: OH/IR – (proto-)planetary nebulae – compact H II regions – infrared radiation – stars: evolution of

1. Introduction

Stars at the AGB are characterized by a very large mass loss rate, which leads to the formation of an optically thick dust shell around the star. It is generally assumed that at the end of the AGB the pulsation of the star will stop and consequently the large mass loss rate or super wind ($\dot{M} > 10^{-5}\ M_\odot\ \mathrm{yr}^{-1}$) will cease as well (e.g. OH 17.7−2.0) (van der Veen et al. 1987). The AGB stars with an oxygen rich dust shell will usually exhibit one or more of the OH 18 cm maser lines (1612 MHz, 1665 MHz, 1667 MHz and/or 1720 MHz) (see for a recent review Habing et al. 1989). The flux ratio between the different maser lines depends strongly on the temperature and density of the dust/gas envelope of the star. The most common and strongest of the maser lines in stellar envelopes is the OH 1612 MHz maser line, which can be observed from the start of the super-wind phase (te Lintel Hekkert 1990) until the planetary nebula phase. During this transition the dust shell will move away from the star and its temperature will decrease from 400 K to about 100 K, when the shell is dispersed (Bedijn 1987). Sun & Kwok (1987) show that after the star has moved off the AGB the 1612 MHz maser line will remain observable for a period of ~100 to 1000 yr, at which point the density in the stellar evelope is too low to support the maser. Lewis (1989) reviews the presence of the different masers in the circumstellar shell as the star moves along the AGB.

Shortly after leaving the AGB the central star will start to ionize the gas in the inner part of the circumstellar shell. During some part of the short transition phase the object will exhibit both continuum radiation from the ionized inner regions and OH maser emission from the (still) neutral outer region (e.g. Zijlstra et al. 1989). During most of the preceding phase on the AGB the 1612 MHz maser line will be the only one detectable; the main lines are either suppressed by competitive gain by the outer 1612 MHz emitting shell (Field 1985; Zijlstra et al. 1989) or collisionally de-excited during the super wind phase. After the star has left the super wind phase it is expected (and observed) that the stars have detectable main-line masers again (Lewis 1989).

Since a large percentage of the planetary nebulae are non-spherical whereas the OH/IR stars, for which VLA or Merlin maps are available, have a spherical stellar envelope, it is expected that the change of geometry will occur during the transition phase of AGB to planetary nebula. The shape of the OH maser line profile, which will no longer show the standard two peak profile, can be used as a test for the geometry (Olnon 1977; Reid et al. 1977).

Summarizing: oxygen rich transition objects between AGB and planetary nebula can be characterized by a far infrared colour temperature between ~200 K and ~100 K, by main-line emission and possibly by 1612 MHz emission with an irregular line profile.

Among the known OH/IR stars several objects have been recognized as possible PPN: e.g. OH 231.8+4.2 (Morris et al. 1987 and references therein), IRAS 16342−3814 and IRAS 15405−4945 (Likkel & Morris 1988; te Lintel Hekkert et al. 1988). These three sources have almost identical IRAS colours; their far infrared flux densities can be fitted with a 100 K (±15 K) black body. All three show main-line and 1612 MHz maser emission, with non-standard profiles and high expansion velocities. This can be interpreted as evidence for a rapid change of the geometry from spherical to bipolar. VLA line observations of the three objects show that the three sources are bipolar (te Lintel Hekkert et al. 1991).

* Present address: Mt Stromlo and Siding Spring Observatories, Private Bag, Weston P.O., ACT 2611, Australia

In this article we present an OH survey intended to find PPN from an IRAS point source catalogue (hereafter PSC) based sample, selected on the assumption that the colour temperatures of PPN are about 100 K.

2. The observations

The observations were carried out with the Nançay radio telescope in July 1988. The half-power beamwidth was 3'.5 in right ascension (α) and 18'.0 in declination (δ). The system temperature was about 60 K. The ratio of flux to antenna temperature was taken to be 1.1 Jy K^{-1}. The RMS fluctuations were less than 0.09 Jy. The four OH transitions were observed simultaneously by splitting the 1024 channel autocorrelator into four banks, each bank observing the left circular polarization of one of the frequencies. We used a frequency switching technique in which each bank observed the velocity range -13 to $+225$ km s^{-1}, after which the central frequency was switched to cover the -180 to $+30$ velocity range. The integration time was 20 min per position. No position determination was attempted. The full velocity range observed is -180 to $+225$ km s^{-1}, with a resolution of 0.9 km s^{-1}.

In general, observations of the 1612 MHz transition are seriously hampered by interference caused by the GLONASS satellite system but, fortunately, this time we were lucky enough to get most of our data interference free. Unfortunately the 1720 MHz spectra were affected by strong radar interference, except for K 3−35, which was observed a numer of times for test purposes.

3. The sample

We applied the following selection criteria to the IRAS PSC. The flux quality of the 12, 25 and 60 μm flux had to be at least 2 (IRAS Explanatory Supplement 1985 (hereafter ES), Sect. V.H.5). The colour selection criteria were: (see also Fig. 3): $0.6 < \log(f_{25\mu m}/f_{12\mu m}) < 1.3$, $\log(f_{60\mu m}/f_{25\mu m}) > -0.05$ and $\log(f_{100\mu m}/f_{60\mu m}) > -0.55$. The Nançay telescope cannot observe sources below $\delta = -40°$. Only sources with $f_{60\mu m} > 30$ Jy were observed.

We further aimed to observe only sources with $|b| > 2°.0$ in order to avoid H II regions and dark clouds. This might introduce a bias in favour of low mass stars and/or local objects.

4. Results

We observed 84 IRAS point sources and detected emission or absorption from 13 of them. Table 1 lists the detected sources, Table 2 the non-detected ones; in Table 3 we give the OH characteristics of the detected sources. Figure 1 shows the OH spectra of the detected sources.

Table 3 also contains a classification of the detected sources based on catalogues available at the Strasbourg data centre ("Centre de Données astronomiques de Strasbourg"). From Table 3 it is clear that we included in the sample a large number of H II regions and star formation regions. OH maser emission is expected during a short period in the life time of a compact H II region (Habing & Israel 1979).

The four stellar objects from Tables 1 and 3 can be classified on basis of the occurrence and character of the OH emission. The existence of both 1612 MHz and 1667 MHz maser lines with equal strength and the semi-irregular shape of the maser profiles (see 5.12) makes IRAS 22036+5306 typical for the evolution scenario as outlined in the introduction (see Sect. 1). The large velocity extent (close to 200 km s^{-1}) of the 1667 MHz maser emission puts IRAS 18491−0207 in the same category as OH 231.8+4.2 and IRAS 15405−4945: high expansion outflow sources, possibly PPN. The classification of Hen 3−1475 (IRAS 17423−1755) is tentative.

5. Individual sources with detected OH lines

5.1. W3(N) (IRAS 02230+6202)

The position of IRAS 02230+6202 shows narrow absorption at all three OH transitions. The absorption originates in the W3 interstellar dust cloud, since -43 km s^{-1} is the velocity of CO in the vicinity of the H II region (Thronson et al. 1985).

Table 1. The IRAS point sources detected in OH

No.	IRAS name	l [°]	b [°]	$f_{60\mu m}$ [Jy]	R31	LRS	Variation (%)	Name
1	02230+6202	133.°783	1.°420	$0.229\,10^4$	1.507		7	W3(N)
2	04361+2547	173.853	−13.746	$0.444\,10^2$	1.390		58	
3	16235−2416	353.093	16.896	$0.220\,10^4$	1.796		0	ρ Oph SL
4	17258−3637	351.632	−1.252	$0.128\,10^5$	1.980		0	G 351.60−1.30
5	17423−1755	9.364	5.779	$0.633\,10^2$	0.951		34	Hen 3−1475
6	18276−1431	17.684	−2.033	$0.120\,10^3$	0.723	5	21	OH 17.7−2.0
7	18491−0207	31.129	−1.019	$0.130\,10^3$	1.371	39	98	
8	19255+2123	56.095	2.095	$0.479\,10^2$	1.291		8	K 3−35
9	19598+3324	70.293	1.601	$0.106\,10^5$	1.545	72	52	K 3−50
10	20197+3721	75.834	0.401	$0.742\,10^4$	1.243		0	G 75.84+0.40
11	21413+5442	98.035	1.446	$0.114\,10^4$	1.373		0	Lynds 1084
12	22036+5306	99.634	−1.836	$0.107\,10^3$	1.102	51	5	
13	22543+6145	109.874	2.115	$0.128\,10^5$	3.054		9	Cep A

Note: The position information is taken from the IRAS point source catalogue.

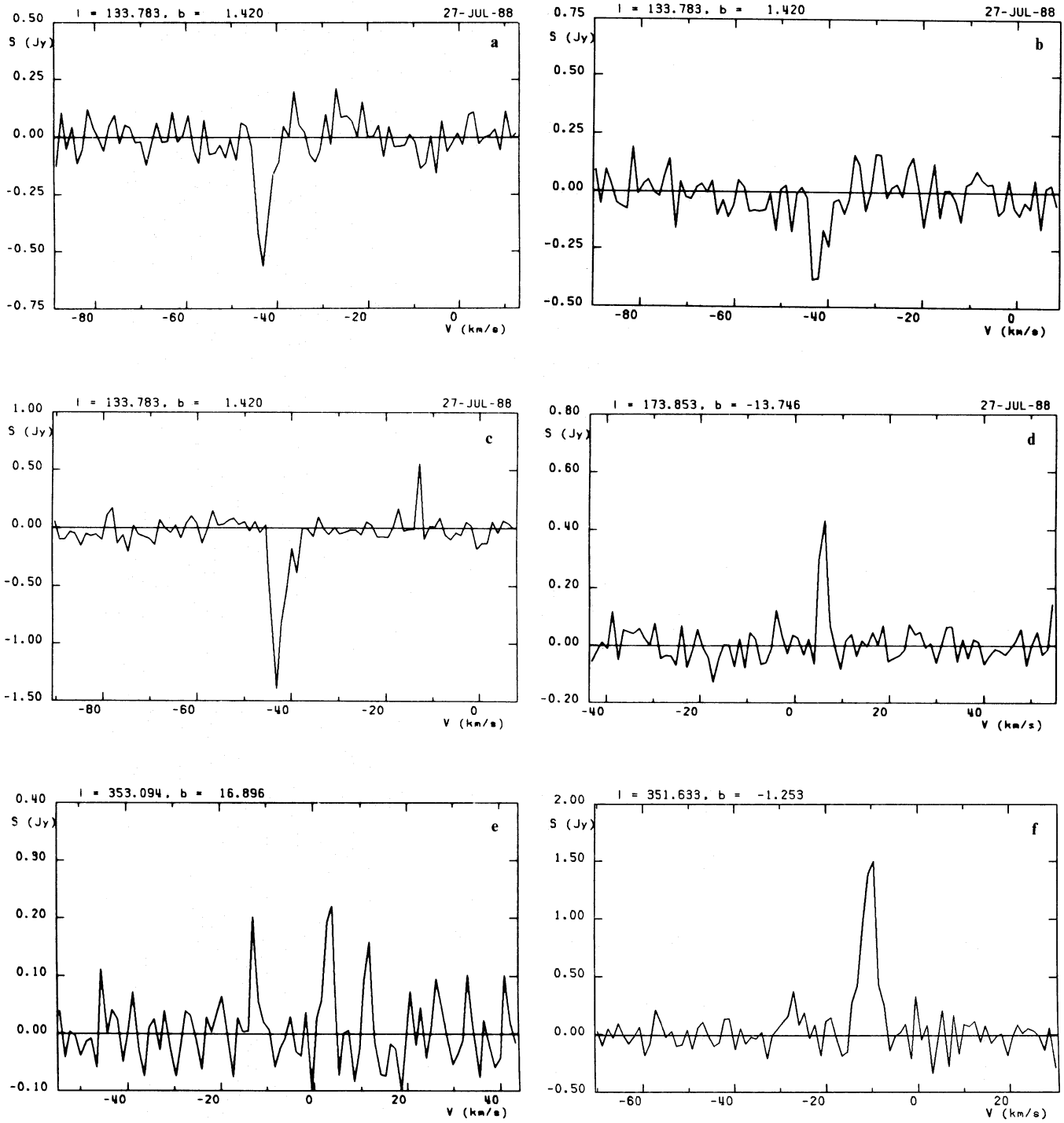

Fig. 1. **a** The OH 1612 MHz profile of W3(N) (IRAS 02230+6202); **b** The OH 1665 MHz profile of W3(N) (IRAS 02230+6202); **c** The OH 1667 MHz profile of W3(N) (IRAS 02230+6202); **d** The OH 1667 MHz profile of IRAS 04361+2547; **e** The OH 1667 MHz profile of ρ Oph SL (IRAS 16235−2416); **f** The OH 1612 MHz profile of G 351.60−1.30 (IRAS 17258−3637); **g** The OH 1665 MHz profile of G 351.60−1.30 (IRAS 17258−3637); **h** The OH 1667 MHz profile of G 351.60−1.30 (IRAS 17258−3637); **i** The OH 1667 MHz profile of Hen 3−1475 (IRAS 17423−1755); **j** The OH 1612 MHz profile of OH 17.7−2.0 (IRAS 18275−1431); **k** The OH 1667 MHz profile of OH 17.7−2.0 (IRAS 18276−1431); **l** The OH 1667 MHz (left circular polarization) profile of IRAS 18491−0207; **m** The OH 1667 MHz (right circular polarization) profile of IRAS 18491−0207; **n** The OH 1612 MHz profile of K 3−35 (IRAS 19255+2123); **o** The OH 1720 MHz profile of K 3−35 (IRAS 19255+2123); **p** The OH 1665 MHz profile of K 3−50 (IRAS 19598+3324); **q** The OH 1667 MHz profile of K 3−50 (IRAS 19598+3324); **r** The OH 1665 MHz profile of G 75.84+0.40 (IRAS 20197+3721); **s** The OH 1667 MHz profile of G 75.84+0.40 (IRAS 20197+3721); **t** The OH 1612 MHz profile of Lynds 1084 (IRAS 21413+5442); **u** The OH 1665 MHz profile of Lynds 1084 (IRAS 21413+5442); **v** The OH 1612 MHz profile of IRAS 22036+5306; **w** The OH 1667 MHz profile of IRAS 22036+5306; **x** The OH 1612 MHz profile of Cep A (IRAS 22543+6145); **y** The OH 1665 MHz profile of Cep A (IRAS 22543+6145); **z** The OH 1667 MHz profile of Cep A (IRAS 22543+6145)

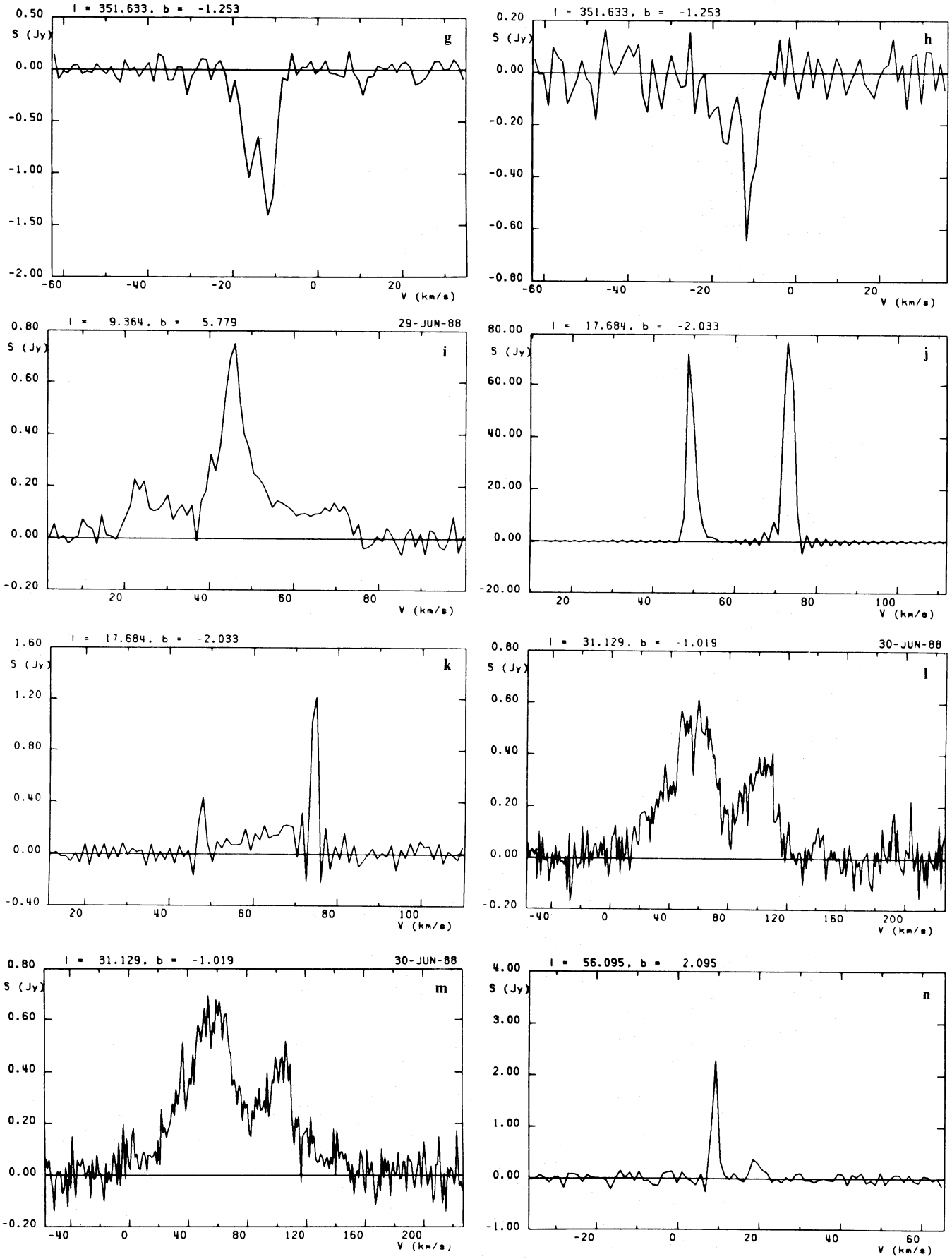

Fig. 1a–z (continued)

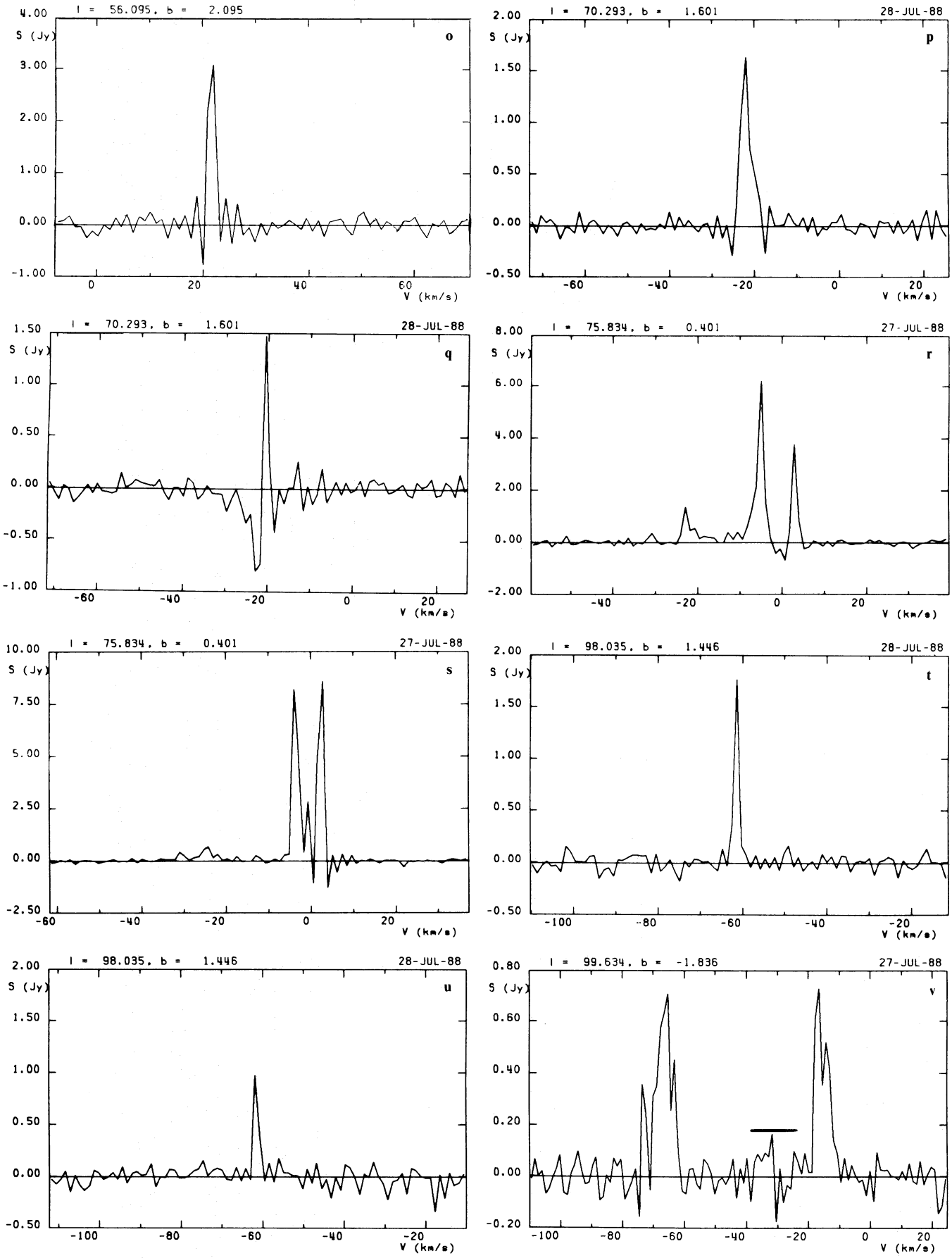

Fig. 1a–z (continued)

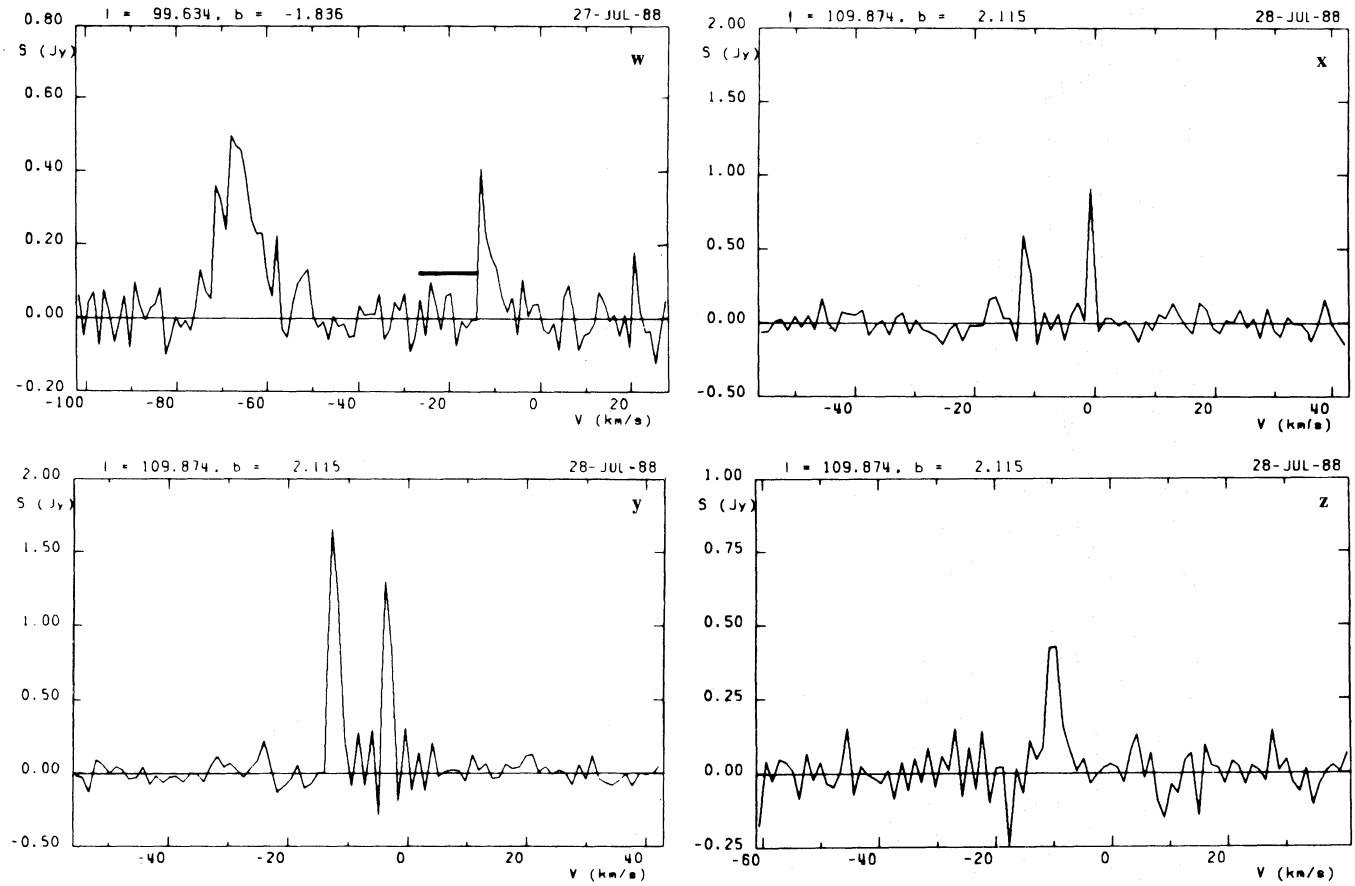

Fig. 1a–z (continued)

Table 2. The IRAS point sources not detected in OH

IRAS name	l [°]	b [°]	$f_{60\mu m}$ [Jy]	R31	LRS	Variation (%)	Name
01174+6110	126.429	−1.234	$0.336\,10^2$	0.914		2	
01202+6133	126.713	−0.822	$0.881\,10^3$	1.924		28	
02044+6031	132.157	−0.726	$0.388\,10^3$	1.506	91	6	RAFGL 5066
02395+6244	135.278	2.797	$0.255\,10^3$	1.369		7	RAFGL 5077
02413+6037	136.357	0.958	$0.766\,10^2$	1.521		0	Lynds 1375
03035+5819	139.912	0.199	$0.106\,10^4$	1.534	81	13	RAFGL 437
04315−0840	204.452	−34.381	$0.332\,10^2$	1.378		17	N1614
04324+5106	154.347	2.606	$0.649\,10^3$	1.715	80	69	RAFGL 5124
06319+0415	207.265	−1.808	$0.959\,10^3$	1.087	53	36	RAFGL 961
07311−2204	237.318	−1.280	$0.218\,10^3$	1.691		35	RAFGL 5235
07396−1805	234.838	2.421	$0.431\,10^2$	1.077		19	PK 234+2°1
07530−3441	250.646	−3.480	$0.848\,10^2$	1.654		0	
08008−3423	251.232	−1.956	$0.928\,10^2$	1.505			
08159−3543	254.056	−0.095	$0.196\,10^3$	1.531		17	
08189−3602	254.660	0.205	$0.178\,10^4$	1.521	92	17	PK 254+ 0°1
08440+1803	208.558	33.289	$0.893\,10^2$	1.625		46	ABELL30
11257+5850	141.906	55.405	$0.105\,10^3$	1.449		50	I0694
12038+5259	138.081	63.072	$0.470\,10^2$	1.508		0	N4102
12243−0036	290.061	61.377	$0.435\,10^2$	1.665		0	M+00−32−012
12540+5708	121.612	60.242	$0.333\,10^2$	1.262		0	A1254+57

Table 2 (continued)

IRAS name	l [°]	b [°]	$f_{60\,\mu m}$ [Jy]	R31	LRS	Variation (%)	Name
13370−3123	314.857	30.106	$0.309\,10^2$	1.077		12	Z CEN
15327+2340	36.627	53.031	$0.104\,10^3$	2.332		17	U09913
15467−2914	343.300	19.174	$0.361\,10^2$	1.468		5	M−05−37−003
16032−3537	341.547	12.106	$0.473\,10^2$	1.817		0	
16288−2450	353.500	15.614	$0.659\,10^2$	1.265		11	
16423+2353	43.108	37.760	$0.346\,10^2$	1.223		9	NGC 6210
17136−3617	350.503	0.956	$0.109\,10^5$	1.645		16	G350.524
17180−2708	358.535	5.471	$0.318\,10^2$	1.128	94	0	PK 358+5°1
17207−3404	353.157	1.052	$0.631\,10^3$	1.580		19	
17262−2343	2.431	5.848	$0.109\,10^3$	1.079	95	2	PK 2+5°1
17462−1959	8.075	3.905	$0.441\,10^2$	1.465		6	PK 8+3°1
17521−2144	7.274	1.845	$0.310\,10^2$	1.215		22	
17584+6638A	96.475	29.967	$0.133\,10^3$	1.248	94	47	RAFGL 5429
18226−2313	9.407	−5.050	$0.368\,10^2$	1.156		7	PK 9−5°1
18236−1241	18.836	−0.303	$0.355\,10^3$	1.990		2	
18372−0537	26.645	0.017	$0.300\,10^3$	1.720			
18454+0250[a]	35.126	2.087	$0.361\,10^2$	0.931		2	
19075+0432[b]	39.160	−2.008	$0.316\,10^2$	0.779		1	
19158+0141	37.601	−5.163	$0.404\,10^2$	0.907		2	V605 AQL
19172+1511	49.694	0.863	$0.806\,10^2$	1.686		36	
19434+5024	83.563	12.791	$0.464\,10^2$	0.972		8	NGC 6826
19560+3135	68.342	1.313	$0.103\,10^3$	1.629		13	
19572+3119	68.238	0.959	$0.479\,10^2$	1.490		1	AS 374
19579+3509	71.576	2.868	$0.442\,10^2$	1.695		7	RAFGL 5453S
20011+3024	67.909	−0.250	$0.368\,10^2$	1.338		0	PK 67−0°1
20103+3419	72.245	0.263	$0.348\,10^2$	1.481		1	
20119+2924	68.349	−2.738	$0.387\,10^2$	0.929		0	PK 68−2°1
20151+3911	76.831	2.187	$0.918\,10^2$	1.748		23	
20178+4046	78.436	2.658	$0.174\,10^4$	1.609		3	
20264+4042	79.308	1.296	$0.233\,10^4$	1.822		6	RAFGL 2586
20298+4013	79.301	0.479	$0.665\,10^2$	1.250			
20310+3741	77.403	−1.212	$0.353\,10^2$	1.281		23	
20332+4124	80.633	0.683	$0.909\,10^3$	1.902		47	
20404+4527	84.649	2.126	$0.319\,10^2$	1.611		0	
20590+5420	93.413	5.494	$0.439\,10^2$	1.466		15	PK 93+5°1
21014−1133	37.761	−34.570	$0.906\,10^2$	1.153	95	4	NGC 7009
21046+4739	89.003	0.375	$0.423\,10^2$	1.246	95	20	DO 39213
21144+5430	95.053	3.972	$0.749\,10^2$	1.795		83	
21190+5140	93.531	1.474	$0.590\,10^3$	1.176	82	6	PK 93+1°1
21266+5016	93.413	−0.357	$0.450\,10^2$	1.444		3	
21340+5339	96.542	1.357	$0.976\,10^2$	1.507		8	
21388+5622	98.856	2.934	$0.529\,10^2$	1.303		99	
21542+5558	100.254	1.278	$0.311\,10^2$	1.083		10	
22142+5206	100.376	−3.580	$0.171\,10^3$	0.915		0	
22176+6303	106.797	5.312	$0.114\,10^5$	1.536	76	7	RAFGL 2884
22384+6101	107.843	2.315	$0.493\,10^2$	1.109	94	48	PK 107+2°1
22551+6139	109.924	1.983	$0.899\,10^3$	1.752		23	
23121+5914	110.890	−1.074	$0.364\,10^2$	1.418			
23151+5912	111.236	−1.238	$0.111\,10^4$	1.339	39	20	
23185+6055	112.226	0.226	$0.433\,10^3$	1.180	51	77	MPCAS
23545+6508	117.315	3.142	$0.756\,10^3$	1.522		0	RAFGL 5623

Notes to Table 2:
[a] Detected by Likkel (1989): a maser spike at 1667 MHz.
[b] Neither detected by Likkel (1989).
The positions are taken from the IRAS point source catalogue, as well as the other information.

Table 3. OH properties of the detections

No.	IRAS name	Freq. [MHz]	Vel. [km s^{-1}]	S_{OH} [Jy]	Type	Name	Ref.
1	02230+6202	1612	−43	−0.6	H II	W3 (N)	1
		1665	−43	−0.4			
		1667	−43	−1.4			
2	04361+2547	1667	6.25	0.43	H II		2, 12, 15
3	16235−2416	1667	3.29	0.22	H II	ρ Oph SL	3
		1667	−13.03	0.20			
4	17258−3637	1612	−9	1.5	H II	G 351.60−01.30	4
		1612	−27.0	0.4			
		1665	−11.7	−0.6			
		1667	−11.7	−1.4			
5	17423−1755	1667	21.5	0.3	PPN	Hen 3−1475	5
		1667	46.0	0.7			
		1667	72.9	0.1			
6	18276−1431	1612	72.8	76.7	PPN	OH 17.7−2.0	6, 7
		1612	48.4	72.2			
		1667	74.6	1.2			
		1667	47.9	0.4			
7	18491−0207	1667	60.0	0.6	PPN		
8	19255+2123	1612	18.6	0.6	H II	K 3−35	8, 16
		1612	8.9	2.3			
		1720	18.6	0.4			
9	19598+3324	1665	−22.0	1.6	H II	K 3−50, ON 3	9, 13
		1667	−21.0	1.5			
10	20197+3721	1665	2.7	8.6	H II	G 75.84+0.40, ON 2	10, 13
		1665	−31.3	0.4			
		1667	2.9	3.8			
		1667	−22.9	1.4			
11	21413+5442	1612	−62.0	1.0	H II	Lynds 1084	11
		1665	−61.5	1.8			
12	22036+5306	1612	−16.6	0.7	PPN		
		1612	−65.6	0.7			
		1667	~ -13.0[a]	$\gtrsim 0.4$[a]			
		1667	−68.0	0.5			
13	22543+6145	1612	−10	0.4	H II	Cep A	14
		1665	−0.7	0.9			
		1665	−12	0.6			
		1667	−4	1.3			
		1667	−13	1.7			

[a] Due to the frequency switching mode we employed, part of the 1667 MHz spectrum was lost.

References: (1) Snell et al. 1988; (2) Heyer et al. 1987; (3) Wouterloot et al. 1984; (4) Brand et al. 1984; (5) Wackerling 1970; Stephenson & Sanduleak 1971; (6) van der Veen et al. 1987; (7) Volk & Kwok 1989; (8) Engels et al. 1985; (9) Fich & Blitz 1984; Acker et al. 1987; (10) Wood et al. 1988; (11) Cohen et al. 1988; (12) Zuckerman & Lo 1987; (13) Braz & Epchtein 1983; (14) Wouterloot et al. 1980; (15) Likkel 1989; (16) Aaquist & Kwok 1989.

5.2. *IRAS 04361+2547*

Zuckerman & Lo (1987) report the detection of an H_2O maser from this source at $+11.8$ km s^{-1}. The velocity and width of the OH (1667 MHz) line are similar to those found by Heyer et al. (1987) for a narrow CO line ($+6.2$ km s^{-1} with a width of 2.7 km s^{-1}), therefore it is probable that both originate from the same interstellar cloud surrounding the IRAS point source. We conclude that IRAS 04361+2547 is embedded in a molecular cloud and is likely a pre-main-sequence star. Likkel (1989) report the detection of maser lines at all four 18 cm OH transitions and an H_2O maser at the position of IRAS 04361+2547. We could not confirm her detection at 1612 MHz (0.24 Jy). The 1665 MHz line decreased after its initial decline from 1.8 Jy to 1.3 Jy in the period September 1986–April 1987 to $\sim$0.2 Jy (a 3σ detection) in July 1988 (Table 3). The decline of the maser strength could be linear with time. The 1667 MHz maser strength declined as well: from 2.0 Jy (Sept. 1986) to 0.43 Jy in July 1988 (Table 3). Our

1720 MHz profile does not contain any information. It is unclear whether the velocity difference between the H_2O masers as reported by Likkel (1989) (9.0 ± 0.3 km s^{-1}) and by Zuckerman & Lo (1987) (6.0 ± 2.6 km s^{-1}) is real, although this maser does show rapid variations in strength.

5.3. *ρ Oph SL (IRAS 16235−2416)*

The OH 1667 MHz emission at $+4$ km s^{-1} found at this position originates from the so-called "streamer" of the Ophiuchus complex (Wouterloot 1984). The integrated emission from each of the two other peaks in the spectrum is too small to say anything definite on the reality of these features.

5.4. *IRAS 17258−3637*

High angular resolution observations will have to show whether the OH features observed in the direction of this sources are associated with the IRAS point source, rather than with the surrounding molecular cloud. The absorption at 1665 MHz and 1667 MHz coincides with NH_3 (velocity: -11.1 km s^{-1}, width: 5.9 km s^{-1}; Batchelor et al. 1977). There might be an extra emission peak in the 1612 MHz spectrum at -27.0 km s^{-1}. Scalise et al. (1989) do not find any H_2O emission from this source.

5.5. *Hen 3−1475 (IRAS 17423−1755)*

W.B. Bidelmann suggested to us that the IRAS source is the same as the stellar object (emission line star) Hen 3−1475 (Henize 1976; Stephenson & Sanduleak 1977). Wackerling (1970) assigns the star a B-type. Parthasarathy & Pottasch (1989) classifies the infrared source as a PPN on basis of its far infrared energy distribution, which they find to be similar to those of young planetary nebulae. The OH 1667 MHz emission profile shows a plateau of emission with a fairly sharp peak on top of it and is, in this respect, similar to the 1667 MHz spectrum of OH 231.8+4.2. We suggest that this object is a PPN which is about to ionize its envelope. Subsequent observations of the right hand circular polarization shows that the degree of polarization of the 1667 MHz maser is less than about 5%. Recent VLA observations at 1667 MHz (te Lintel Hekkert et al. 1991) show that the source deviates strongly from spherical symmetry.

5.6. *OH 17.7−2.0 (IRAS 18276−1431)*

This well known object has the warmest dust/gas envelope in our sample. Van der Veen et al. (1987) (see also Volk & Kwok 1989; Trams et al. 1989 and references therein) classify it as a PPN on basis of the OH and far infrared characteristics.

5.7. *IRAS 18491−0207*

The 1667 MHz spectrum of this source is spectacular: a velocity width of 200 km s^{-1}. The profile resembles that of the main-line emission of IRAS 16342−3814. Subsequent observations of the right hand circular polarization have shown that the degree of polarization of the 1667 MHz maser is less then about 5% for the main part of the emission; some peaks at ~ 200 km s^{-1} (if real) are 100% polarized. The peak at $+5$ km s^{-1} has been confirmed. No optical counterpart has been found, neither are there any other measurements known to the authors.

5.8. *K 3−35 (IRAS 19255+2123)*

Engels et al. (1985) detected a 1612 MHz maser and also an H_2O maser and weak 1667 MHz emission. They did not observe the OH 1720 MHz transition. They found three 1612 MHz emission groups: ~ -2, $+9.1$ and $+17$ to $+21$ km s^{-1}. There are two peaks at 1667 MHz: at -4 km s^{-1} and at $+7.8$ km s^{-1}. The H_2O maser emission is just outside the third 1612 MHz ($+17$ to $+21$ km s^{-1}) velocity range, at $+22.2$ to $+24.7$ km s^{-1}. The detection of extended CO emission, probably related to the dark cloud Lynds 755 and at the velocity of one of the 1612 MHz maser peaks, prompted Engels et al. to suggest that K 3−35 is an incorrectly identified planetary nebula and that most likely it is a compact H II region. The presence of the 1720 MHz maser line, which has never been observed in stellar envelopes, confirms this suggestion.

The brightest 1612 MHz maser emission we find is at the same velocity ($+8.9$ km s^{-1}), but only half as bright as in the observations of Engels et al., assuming that the line is not significantly polarized. A similar decrease has probably happened with the 1612 MHz emission at -3 to -1 km s^{-1}, since we could not find any emission with a peak intensity above 0.2 Jy. For the third 1612 MHz emission peak we find a similar flux as Engels et al. The upper limit for the 1667 MHz emission is $+0.2$ Jy, which is half as bright as the intensity found by Engels et al. We detected 1720 MHz maser emission near the velocity of the H_2O maser emission at $+22.1$ km s^{-1}. The decrease in maser strength of the 1612 MHz and 1667 MHz maser spots could be an indication that parts of the envelope or cocoon are "eaten' by the ionization front.

Thus we find that the 1667 MHz and first two groups of the 1612 MHz masers behave similarly, in contrast to the maser emission around $+20$ km s^{-1}. This suggests that there are, at least, two different sources (or two places of interaction) in the vicinity of the IRAS point source. The 2 cm and 6 cm continuum maps made by Aaquist & Kwok (1989) is consisted with this view.

The detection of 1720 MHz maser emission is quite interesting: known 1720 MHz masers are rare and it has been suggested by Andresen (1989) that the 1720 MHz maser line could be pumped by the dissociation of H_2O, which leaves the resulting OH in an excited state. This process will not pump any of the other maser lines. Thus we expect to observe 1720 MHz maser emission at velocities near or at the velocity of H_2O emission, as we indeed observe.

5.9. *K 3−50 (ON3, IRAS 19598+3324)*

This source is discussed in detail by Roelfsema et al. (1988). OH main-line emission was detected by Elldér et al. (1969) (see also Matthews et al. 1986; Braz & Epchtein 1981), although his observations were not sensitive enough to detect the absorption in the 1667 MHz and 1665 MHz spectra. The association between the OH emission and K 3−50 comes from the work by Winnberg et al. (1981) (see also Israel 1976).

5.10. *G 75.84+0.40 (ON2, IRAS 20197+3721)*

Maser emission from this source has been discovered by Winnberg (1970). The 1667 MHz profile has not changed significantly but the 1665 MHz maser emission has changed; the emission peaks at -24 km s^{-1} and -31 km s^{-1} are new.

5.11. Lynds 1084 (IRAS 21413+5442)

This is the only detected source we have in common with Cohen et al. (1988). Since their observations the OH lines have not changed significantly. Scalise et al. (1989) found an H_2O maser at -60.1 km s^{-1}, which is close to the velocities of the OH maser lines.

5.12. IRAS 22036+5306

IRAS 22036+5306 shows the characteristic two peak profile of an expanding stellar circumstellar envelope at both 1612 MHz and 1667 MHz transitions. Zuckerman & Lo (1987) did not find any H_2O emission at this position. This source has very red colours compared to "regular" OH/IR stars. It has been suggested (Sun & Kwok 1987) that these cool OH/IR stars are PPN's, where the mass-loss has recently stopped. Since then the original circumstellar envelope (CSE) has expanded and cooled. We were not able to find an optical counterpart on the Palomar Sky Survey (PSS) plates.

The expansion velocity of IRAS 22036+5306 (24.5 km s^{-1}) is rather high in comparison with other OH/IR stars (te Lintel Hekkert et al. 1989). This could be the start of the fast wind as observed in IRAS 18491−0207 and IRAS 16342−3814. The one to one ratio of the 1612 MHz and 1667 MHz maser intensities is in accordance with the scenario by Lewis (1989) for the re-appearance of the main line emission after the AGB phase. The absence of an H_2O maser is consistent with this interpretation as well.

The OH and IRAS characteristics suggest that this source has recently left the AGB and could be in a phase of rapid evolution.

5.13. Cep A (IRAS 22543+6145)

The OH main lines of this source have been discussed by Wouterloot et al. (1980). Although the velocity resolution of our observations is lower than those of Wouterloot et al. it is clear that the spectrum has changed significantly between the two epochs. Wouterloot & Walmsley (1986) detected H_2O masers at several velocities (-37 km s^{-1} to $+17$ km s^{-1}) for this source.

Cohen et al. (1984) review the object. In 1985 it experienced an outburst (Cohen et al. 1985). Comparing our spectra with those from Cohen it is clear that the outburst also disrupted the masers. Only one of the many maser lines from 1985 can be seen in Fig. 1. The 1665 MHz maser at ~ -1 km s^{-1} has not been detected previously. New Merlin observations might reveal the growth of the H II region into the surrounding cloud.

6. The detection statistics

Figure 2 shows the number of detected and non-detected sources per bin as function of $f_{60\mu m}$. It is apparent from the figure that the detections fall in two groups. The sources with fluxes over 1,000 Jy at 60 μm are H II regions that can be associated with dark clouds and/or star formation regions. The group of sources with $f_{60\mu m}$ less then 1,000 Jy consists of PPNs plus the two H II regions IRAS 04361+2547 and K 3−35; the latter sources are the two in the first flux bin. It is clear that the H II regions IRAS 04361+2547 and K 3−35 are of a different nature than the other H II regions, since they have $f_{60\mu m}$ fluxes 2 orders of magnitude

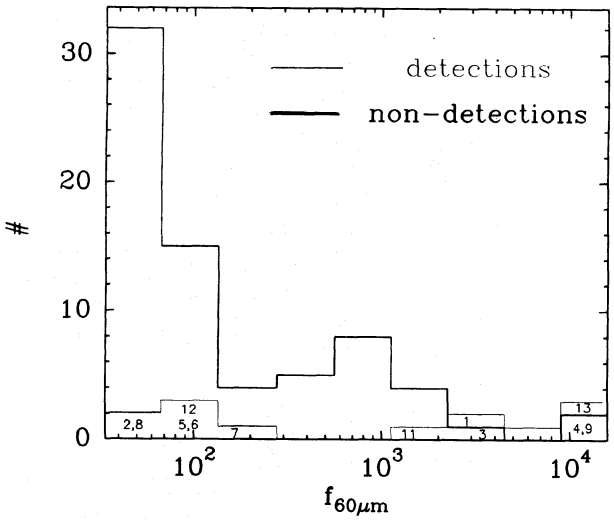

Fig. 2. The number of detected and the number of non-detected IRAS sources per bin as function of $f_{60\mu m}$ (Jy). The numbers in the bins correspond with the source numbers in Tables 1 and 3. Sources 2 and 8 are two low luminosity H II regions IRAS 04361+2547 and K 3−50. Sources 5, 6, 7 and 12 are the stellar sources of Table 3. The sources 1, 3, 4, 9, 11 are H II regions, which are embedded in dark clouds

smaller than the other H II regions, and yet OH masers of comparable flux.

The detection rate for the sources with $f_{60\mu m} > 1{,}000$ Jy is 50% (7 detections out of 14 observations). This is significantly higher than what was found by Cohen et al. (1989): 22%. Cohen et al. performed a main-line OH survey, on a selection of IRAS sources with similar ($f_{60\mu m}/f_{25\mu m}$) colours. They observed sources close to the galactic plane at $|b| \lesssim 1.^\circ 5$ with $f_{100\mu m} > 1000$ Jy and $f_{60\mu m} > 1000$ Jy. Since our sample is more biased towards sources with $f_{60\mu m} > f_{100\mu m}$ in comparison with their sample, the difference in detection rate is consistent with the conclusion of Cohen et al. that the maser souces are, on average, warmer in the 60 μm/100 μm colour temperature than the non-maser sources.

Assuming an infrared bolometric correction of BC=10 (for a dust-shell temperature of 100 K; BC is defined by: $f_{int} = BC \times \nu f_{\nu=12\mu m}$) (van der Veen & Breukers 1989) we expect $f_{60\mu m}$ between 40 Jy and 80 Jy for an AGB star with an infrared luminosity of 5,000 $L_\odot$ to 10,000 $L_\odot$ (Habing 1986) at a distance of 4.4 kpc from the sun. Analogous to the sample of te Lintel Hekkert et al. 1991, we assume that that completeness limit for our sample is 3 Jy at 12 μm. This corresponds to a distance of 4.4 kpc for the assumed luminosity. On basis of these rather general assumptions we can expect to find the stars in the $f_{60\mu m}$ bins of 60 Jy to 256 Jy (second and third bin of Fig. 2). It is quite likely that the PPN's have non-spherical dust shells, which may increase BC, and decrease the limiting distance and $f_{60\mu m}$.

Figure 3a shows the colour-colour diagram based on $f_{12\mu m}$, $f_{25\mu m}$ and $f_{60\mu m}$ bands for the observed sources (the numbers in the figure refer to Tables 1 and 3). Figure 3b shows the colour-colour diagram based on $f_{25\mu m}$, $f_{60\mu m}$ and $f_{100\mu m}$ bands for the observed sources. Although, on average the PPN have warmer colours than the H II regions (except for the two H II regions IRAS 04361+2547 and K 3−35) there is no way to improve our

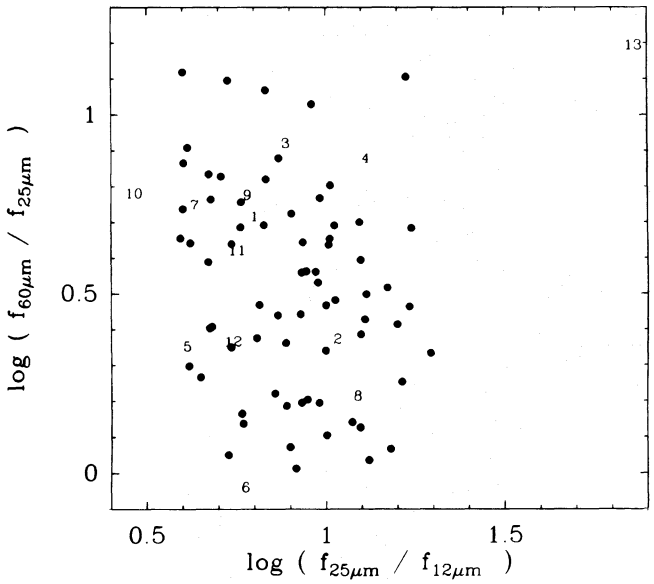

Fig. 3a. The colour-colour diagram based on $f_{12\mu m}$, $f_{25\mu m}$ and $f_{60\mu m}$ bands for the observed sources; the numbers in the figure correspond to the detected sources in Tables 1 and 3. The • correspond with the non-detections listed in Table 2

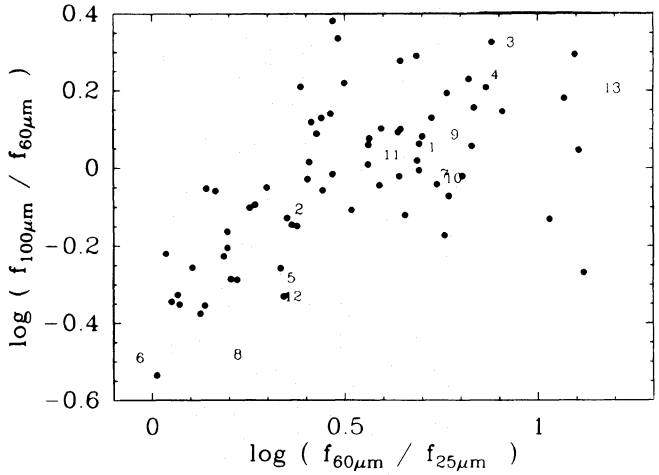

Fig. 3b. The colour-colour diagram based on $f_{25\mu m}$, $f_{60\mu m}$ and $f_{100\mu m}$ bands for the observed sources

colour selection criteria in order to discriminate against the H II regions: Nature gave the two groups nearly identical infrared colours, since both groups evolve on similar tracks in the Hertzsprung-Russell diagram. It is clear that the detection rate cannot be improved by other colour selection criteria.

7. Conclusions

The survey was successful in detecting three new PPN. The selection criteria for finding PPN can be refined using $f_{60\mu m}$, but this will not improve the detection rate greatly. The $f_{60\mu m}$ is a good disciminator between PPN and H II regions.

The maser source of K 3−35 is a good candidate for the proposed pumping mechanism for the 1720 MHz maser line by photo-dissociation of H_2O.

High angular resolution observations of both H II regions and PPN are needed to provide information on geometry and dynamics of the dust and gas envelope.

Acknowledgements. PLH gratefully acknowledges the hospitality of the staff at Nançay. My special thanks go to Dr. W.B. Bidelmann for pointing out to me that IRAS 17423−1755 and Hen 3−1475 are one and the same object. I am happy to acknowledge the interest of Drs. Albert Zijlstra, Phil Maloney, Harm Habing, Anders Winnberg and Friso Olnon for this project and their critical reading of the manuscript. Some of the associations of the detected IRAS sources are based on the SIMBAD data retrieval system, database of the Strasbourg, France, astonomical Data Center.

References

Aaquist O.B., Kwok S., 1989, A&A 222, 227
Acker A., Chopinet M., Pottasch S.R., Stenholm B., 1987, A&AS 71, 163
Andresen P., 1986, A&A 154, 42
Batchelor R.A., Gardner F.F., Knowles S.H., Mebold U., 1982, Proc. Astron. Soc. Aust. 3, 152
Bedijn P.J., 1987, A&A 186, 136
Brand J., van der Bij M.P.D., de Vries C.P., Israel F.P., de Graauw T., van de Stadt H., Wouterloot J.G.A., Leene A., Habing H.J., 1984, A&A 139, 181
Braz A., Epchtein N., 1981, A&AS 54, 167
Carter J.C., 1986, Haystack Observatory Internal Report on "Glonass Observations"
Cohen R.J., Rowland P.R., Blair M.M., 1984, MNRAS 210, 425
Cohen R.J., Brebner G.C., 1985, MNRAS 216, 51p
Cohen R.J., Baart E.E., Jonas J.L., 1988, MNRAS 231, 205
Cohen R.J., 1989, Rep. Prog. Phys. 52, 881
Elldér J., Rönnäng B., Winnberg A., 1969, Nat 222, 67
Engels D., Schmid-Burgk J., Walmsley C.M., Winnberg A., 1985, A&A 148, 344
Fich M., Blitz L., 1984, ApJ 279, 125
Field D., 1985, MNRAS 217, 1
Habing H.J., te Lintel Hekkert P., van der Veen W.E.C.J., 1989, in: Planetary Nebulae, ed. Torres-Peimbert, Reidel, Dordrecht, p 359
Henize K.G., 1976, ApJS 30, 491
Heyer M.H., Snell R.L., Goldsmith P.F., 1987, ApJ 321, 370
Israel F.P., 1976, A&A 48, 193
Krugel E., Densing R., Nett H., Roser H.P., Schafer F., Schmid-Burgk J., Schwaab G., van der Wal P., Wattenbach R., 1989, A&A 211, 419
Lewis B.M., 1989, ApJ 338, 234
Likkel L., 1989, ApJ 344, 350
Likkel L., Morris M., 1988, ApJ 329, 914
te Lintel Hekkert P., 1990, Thesis, Leiden University
te Lintel Hekkert P., Caswell J.L., Habing H.J., Norris R.P., Haynes R.F., 1988, A&A 202, L19
te Lintel Hekkert P., Zijlstra A.A., Likkel L., Cohen R.J., 1991 (in preparation)
te Lintel Hekkert P., Caswell J.L., Habing H.J., Norris R.P., Haynes R.F., 1991, A&A (in press)

Matthews H.E., Baudry A., Guilloteau S., Winnberg A., 1986, A&A 163, 177
Morris M., Guilloteau S., Lucas R., Omont A., 1987, ApJ 321, 888
Olnon F.M., 1977, Thesis Leiden University
Parthasarathy M., Pottasch S.R., 1989, A&A 225, 521
Reid M.J., Muhleman D.O., Moran J.M., Johnston K.J., Schwarz P.R., 1977, ApJ 214, 60
Roelfsema P.R., Goss W.M., Geballe T.R., 1988, A&A 207, 132
Sun J., Kwok S., 1987, A&A 185, 285
Scalise Jr. E., Rodríguez L.F., Mendoza-Torres E., 1989, A&A 221, 105
Snell R.L., Huang Y.-L., Dickman R.L., Claussen M.J., 1988, ApJ 325, 853
Stephenson C.B., Sanduleak N., 1977, Warner & Swaney Obs. Publ. 2, No. 4, 1
Thronson Jr. H.A., Schwartz P.R., Smith H.A., Lada C.J., Glaccum W., Harper D.A., 1984, ApJ 297, 662
Trams N.R., Waters L.B.F.M., Waelkens C., Lamers H.J.G.L.M., van der Veen W.E.C.J., 1989, A&A 218, L1
van der Veen W.E.C.J., Habing H.J., Geballe T., 1987, in: Planetary and Proto-planetary nebulae: from IRAS to ISO, 69
van der Veen W.E.C.J., Breukers R.J.L.H., 1989, A&A 213, 133
Volk K.M., Kwok S., 1989, ApJ 342, 345
Wackerling L.R., 1970, Mem. R. Astron. Soc. 73, 153
Winnberg A., 1970, A&A 9, 259
Winnberg A., Terzides Ch., Matthews H.E., 1981, AJ 86, 410
Wood D.O.S., Handa T., Fukui Y., Churchwell E., Sofue Y., Iwata T., 1988, ApJ 326, 884
Wouterloot J.G.A., Habing H.J., Herman J., 1980, A&A 120, L11
Wouterloot J.G.A., 1984, A&A 135, 32
Wouterloot J.G.A., Walmsley C.M., 1986, A&A 168, 237
Zuckerman B., Lo K.Y., 1987, A&A 173, 263
Zijlstra A.A., te Lintel Hekkert P., Pottasch S.R., Caswell J.L., Mezak Ratag, Habing H.J., 1989, A&A 217, 157